ISSN 2472-1972

Male Mice Lacking NLRX1 Are Partially Protected From High-Fat Diet–Induced Hyperglycemia

Sheila R. Costford,[1,2] Ivan Tattoli,[1] Francis T. Duan,[1] Allen Volchuk,[1,2] Amira Klip,[1,2] Dana J. Philpott,[1] Minna Woo,[1,3] and Stephen E. Girardin[1]

[1]University of Toronto, Toronto, Ontario M5S 1A1, Canada; [2]The Hospital for Sick Children, Toronto, Ontario M5G 1X8,Canada; and [3]Toronto General Research Institute, University Health Network, Toronto, Ontario M5G 1L7, Canada

Nod-like receptor (NLR)X1 is an NLR family protein that localizes to the mitochondrial matrix and modulates reactive oxygen species production, possibly by directly interacting with the electron transport chain. Recent work demonstrated that cells lacking NLRX1 have higher oxygen consumption but lower levels of adenosine triphosphate, suggesting that NLRX1 might prevent uncoupling of oxidative phosphorylation. We therefore hypothesized that NLRX1 might regulate whole-body energy metabolism through its effect on mitochondria. Male NLRX1 whole-body knockout (KO) mice and wild-type (WT) C57BL/6N controls were fed a low-fat or a high-fat (HF) diet for 16 weeks from weaning. Contrary to this hypothesis, there were no differences in body weight, adiposity, energy intake, or energy expenditure between HF-fed KO and WT mice, but instead HF KO mice were partially protected from the development of diet-induced hyperglycemia. Additionally, HF KO mice did not present with hyperinsulinemia during the glucose tolerance test, as did HF WT mice. There were no genotype differences in insulin tolerance, which led us to consider a pancreatic phenotype. Histology revealed that KO mice were protected from HF-induced pancreatic lipid accumulation, suggesting a potential role for NLRX1 in pancreatic dysfunction during the development diet-induced type 2 diabetes mellitus. Hence, NLRX1 depletion partially protects against postabsorptive hyperglycemia in obesity that may be linked to the prevention of pancreatic lipid accumulation. Although the actual mechanisms restoring glucose and insulin dynamics remain unknown, NLRX1 emerges as a potentially interesting target to inhibit for the prevention of type 2 diabetes mellitus.

Freeform/Key Words: ectopic lipid, glucose-stimulated insulin secretion, NLRX1, type 2 diabetes mellitus

Nod-like receptor (NLR)X1 is a member of the NLR family [1] whose function is poorly understood. Targeted to the mitochondrial matrix [2–4], NLRX1 interacts with UQCRC2, a component of complex III of the electron transport chain (ETC) [1, 5]. The ETC accepts electrons from reducing equivalents NADH and $FADH_2$, which are generated by the tricarboxylic acid cycle. As the electrons are passed from complex to complex within the chain, protons are pumped from the matrix side of the mitochondrial inner membrane into the intermembrane space, creating an electrochemical gradient. Protons return to the matrix through adenosine triphosphate (ATP) synthase, and energy is captured in the form of ATP. Increased potential across the mitochondrial inner membrane leads to increased production of reactive oxygen species (ROS), which act as important signaling molecules within the cell,

Abbreviations: ANOVA, analysis of variance; ATP, adenosine triphosphate; ETC, electron transport chain; GSIS, glucose-stimulated insulin secretion; GTT, glucose tolerance test; HF, high-fat; IP, intraperitoneal; ITT, insulin tolerance test; KO, knockout; LF, low-fat; NLR, Nod-like receptor; RER, respiratory exchange ratio; ROS, reactive oxygen species; SEM, standard error of the mean; T2DM, type 2 diabetes mellitus; UCP, uncoupling protein; VCO_2, carbon dioxide production; VO_2, oxygen consumption; WT, wild-type.

Received 6 September 2017
Accepted 16 February 2018
First Published Online 21 February 2018

but can be damaging to cellular components at high levels. A negative feedback loop exists whereby certain species of ROS (*i.e.*, superoxide and 4-hydroxy-2-nonenal) activate uncoupling proteins residing in the mitochondrial inner membrane [6–8]. These proteins uncouple oxidative phosphorylation by allowing protons to leak back across the inner membrane into the matrix, thereby reducing the membrane potential and mitigating ROS production. Because protons are not returning to the matrix via ATP synthase, energy is dissipated as heat instead of being captured by ATP. Targeting this energy-wasting system has been proposed as a means of treating obesity (reviewed in [9]). ROS are produced mainly at complex I and complex III of the ETC, but superoxide generated at complex III is released both into the intermembrane space as well as into the mitochondrial matrix [10–12]. Interestingly, overexpression of NLRX1 results in increased ROS production [13] whereas ablation of NLRX1 attenuates tonic ROS levels in transformed mouse embryonic fibroblasts [14]. Additionally, NLRX1 was shown to enhance ROS produced in response to *Chlamydia* [15], viral infection [16], and tumor necrosis factor stimulation [17]. Alternatively, increased superoxide levels were observed in NLRX1-deficient epithelial kidney cells in the reoxygenation phase in a model of ischemia–reperfusion [18]. These findings suggest a complex mode of ROS regulation by NLRX1 and that the effect of NLRX1 on ROS might be secondary to a more general impact on mitochondrial physiology. In agreement with this, Singh *et al.* [17] demonstrated that NLRX1 inhibited the activity of both complexes I and III of the ETC, suggesting that the effect of NLRX1 on ROS might be indirect and a result of the more global modulation of the ETC and of OXPHOS by NLRX1. In support of these results, we recently demonstrated that cells lacking NLRX1 have increased oxygen consumption but decreased ATP content [18] (*i.e.*, are uncoupled), suggesting that NLRX1 might inhibit, either directly or indirectly, the low level of physiological uncoupling of OXPHOS. If this were the case, we would expect to observe a reduction in body weight and possibly in fat accumulation in NLRX1-deficient mice due to higher uncoupling. To test this hypothesis, we analyzed the effects of high-fat (HF) feeding on male wild-type (WT) and NLRX1 knockout (KO) mice. Surprisingly, although we found no genotype differences in body weight, adiposity, energy intake or energy expenditure, we observed that KO mice were protected from HF diet–induced pancreatic lipid accumulation and hyperglycemia. These results suggest that NLRX1 may be a potential target for the prevention of ectopic accumulation of pancreatic lipid and improved blood glucose homeostasis during a state of overnutrition.

1. Materials and Methods

A. Animals

C57BL/6N mice lacking the *Nlrx1* gene were previously generated by our laboratory [19] and are referred to as NLRX1 KO mice throughout the text. WT littermate C57BL/6N mice from Het × Het crosses were used as controls. Male mice were fed a low-fat (LF; 10% by kcal) defined diet (D12450J, Research Diets, New Brunswick, NJ) or an HF (60% by kcal) defined diet (D12492, Research Diets) for 16 weeks from weaning (at 3 weeks of age). Diets contained equal amounts of sucrose, maltodextrin 10, and soybean oil (% kcal), but varied in their content of cornstarch and lard. Diets were not isocaloric. Mice were individually caged and maintained at 20°C to 24°C with light from 6:00 AM to 8:00 PM. Body weight and energy intake were assessed every week at the same time of day. Fasting blood glucose was measured and plasma was collected after 5, 7, 9, 11, and 13 weeks on the diet. A glucose tolerance test (GTT) and an insulin tolerance test (ITT) were performed after 14 and 15 weeks on the diet, respectively. Indirect calorimetry was performed after 16 weeks on the diet, and then mice were euthanized via cervical dislocation following a 4-hour fast. Tissues were collected and preserved in 10% buffered formalin or OCT compound, or were flash frozen in liquid nitrogen and stored at −80°C for further analysis. Murine studies were approved by the University of Toronto Animal Care Committee.

B. Body Weight and Energy Intake

Mouse body weight and remaining diet were measured on a CLW 201 electronic balance (VWR, Radnor, PA) at 2:00 PM each week of the study.

C. Indirect Calorimetry

Oxygen consumption (VO_2), carbon dioxide production (VCO_2), and ambulatory activity were measured using a comprehensive laboratory animal monitoring system (CLAMS; Columbus Instruments, Columbus, OH). Energy expenditure was measured during 24 hours after a 24-hour acclimation period. The respiratory exchange ratio (RER) was calculated as VCO_2/VO_2. Ambulatory activity was estimated by the number of infrared beam breaks along the *x*-axis of the metabolic cage. Data were analyzed using the comprehensive laboratory animal monitoring system examination tool (CLAX, version 2.2.10; Columbus Instruments).

D. Fasting Glucose and Insulin

After a 4-hour fast, basal blood glucose levels were measured using a Contour glucometer (Bayer, Leverkusen, Germany) by cutting the tip of the tail. Fasting plasma insulin was determined using a high-sensitivity mouse insulin immunoassay kit (Antibody and Immunoassay Services, Li Ka Shing Faculty of Medicine, University of Hong Kong, Pokfulam, Hong Kong), as per the manufacturer's instructions.

E. Glucose and Insulin Tolerance Tests

After a 4-hour fast, baseline blood glucose levels were measured using a Contour glucometer (Bayer) by cutting the tip of the tail. Mice were given an intraperitoneal (IP) injection of 10% sterile glucose (Sigma-Aldrich, St. Louis, MO) equivalent to 1 g of glucose per kilogram body weight or an IP injection of 1.5 U Humulin R U-100 insulin (Eli Lilly and Company, Indianapolis, IN) per kilogram body weight in 0.9% sterile saline. Blood glucose levels were measured at 15, 30, 45, 60, and 90 min postinjection. During the GTT, plasma was collected for determination of insulin at baseline, 15 and 60 minutes postinjection.

F. Histology and Immunohistochemistry

Pancreas tissues preserved in 10% neutral-buffered formalin were embedded in paraffin at the Toronto Centre for Phenogenomics Centre for Modeling Human Disease Pathology Services (Toronto, Canada). The tissues were sectioned longitudinally through the pancreatic head-to-tail axis (5 μm thickness). Three pancreatic sections per mouse, separated by at least 100 μm, were mounted on glass slides. Sections were deparaffinized in xylene, rehydrated in a descending ethanol series, and washed in distilled water. Sections were then incubated in 1% hydrogen peroxide in Tris-buffered saline (pH 7.4) for 15 minutes to block endogenous peroxidase activity. Nonspecific binding of IgG was blocked using normal goat serum diluted 1:50 in Tris-buffered saline for 30 minutes. The slides were incubated with primary antibody overnight at 4°C in a humidity chamber. The following polyclonal antibody was used: guinea pig anti-porcine insulin (1:400) (Dako, Carpinteria, CA; AB_10013624). Sections then were washed three times each for 5 minutes in buffer. Insulin levels were detected by use of the streptavidin–alkaline phosphatase method (Dako) according to the manufacturer's protocol. The slides were counterstained with hematoxylin to identify the morphology of the cells, and were then dehydrated in an ascending series of alcohols, cleared in xylene, and mounted under glass coverslips using Paramount mounting medium (SP15-500, Fisher Scientific, Waltham, MA). To determine the presence of insulin, pancreatic sections were digitally scanned using the Zeiss AxioScan slide scanner, and areas positive for insulin staining were analyzed using Zen Blue desktop image analysis software. Total tissue (blue) and insulin-positive (red) areas were identified and quantified. Hematoxylin and eosin staining was used

to determine pancreatic lipid accumulation because paraffin section preparation removed the lipid droplets from the tissue. Sections were examined at ×200 magnification. Ten slides from each group were included in the quantification and 10 fields were randomly selected on each slide. The areas of the (empty) lipid droplets were measured by tracing around their perimeters.

G. Statistical Analysis

Data are expressed as means ± standard error of the mean (SEM). A two-way analysis of variance (ANOVA) with a Tukey posttest was used to detect differences in data sets containing two variables (*i.e.*, genotype and diet). Statistical significance was set at $P < 0.05$. Graphs were prepared and data were analyzed using GraphPad Prism version 7 (GraphPad Software, La Jolla, CA).

2. Results

A. Body Weight and Adiposity

There were no differences in weaning body weight between any of the groups (Fig. 1A). After 16 weeks on the diets, both HF-fed WT and HF-fed NLRX1 KO mice had higher body weights compared with WT and KO mice fed the LF diet (effect of diet: $F_{1,36} = 34.37$, $P < 0.0001$) (Fig. 1B); however, we found no genotype differences in body weight during the course of the study (Fig. 1C), indicating that NLRX1 does not in fact play a role in the control of body weight during overnutrition. Similarly, although HF-fed WT and KO mice had heavier inguinal white adipose tissue (effect of diet: $F_{1,35} = 43.24$, $P < 0.0001$) and epididymal white adipose tissue (effect of diet: $F_{1,35} = 50.71$, $P < 0.0001$) depots, there were no genotype differences in adiposity (Fig. 1D and 1E). Finally, we detected no diet or genotype differences in brown adipose tissue weight (Fig. 1F).

B. Energy Intake and Energy Expenditure

As expected, HF-fed animals consumed more kilocalories per day compared with LF-fed animals ($F_{3,36} = 30.12$, $P < 0.0001$); however, we observed no genotype differences in energy intake (Fig. 2A) or metabolic efficiency (data not shown) during the course of the study. Similarly, measurements taken for 24 hours during indirect calorimetry revealed no genotype differences in energy or water intake (data not shown). HF-fed animals expended less energy (as measured by VO_2) (effect of diet during light cycle: $F_{1,36} = 22.38$, $P < 0.0001$; effect of diet during dark cycle: $F_{1,36} = 22.25$, $P < 0.0001$) and had lower RERs during both the light (effect of diet: $F_{1,36} = 244.8$, $P < 0.0001$) and dark (effect of diet: $F_{1,36} = 144$, $P < 0.0001$) cycles, but no genotype differences were observed (Fig. 2B–2E). Neither diet nor genotype differences were observed in spontaneous physical activity in terms of total x-axis activity (Fig. 2F and 2G), ambulatory x-axis activity (Fig. 2H and 2I), or z-axis activity (data not shown).

C. Fasting Glucose and Insulin

As expected, HF WT mice became hyperglycemic during the course of the study compared with LF WT controls (over time: $F_{3,36} = 33.16$, $P < 0.0001$; at endpoint: $F_{1,36} = 21.49$, $P < 0.0001$) (Fig. 3A and 3B). Interestingly, HF KO mice developed significantly less hyperglycemia than did HF WT mice ($P < 0.05$) (Fig. 3A and 3B) despite similar body weights (Fig. 1C) and adiposity (Fig. 1D–1F). Moreover, whereas HF WT mice became hyperinsulinemic compared with LF WT controls during the course of the study (over time: $F_{3,36} = 3.534$, $P < 0.05$; at endpoint: $F_{1,36} = 8.46$, $P < 0.01$), insulin levels in HF KO mice were not significantly higher than those in LF-fed mice (Fig. 3C and 3D).

D. Glucose and Insulin Tolerance

HF WT and HF KO mice had significantly higher blood glucose during the GTT compared with LF WT and LF KO mice, respectively ($F_{3,36} = 19.53$, $P < 0.0001$) (Fig. 4A). There

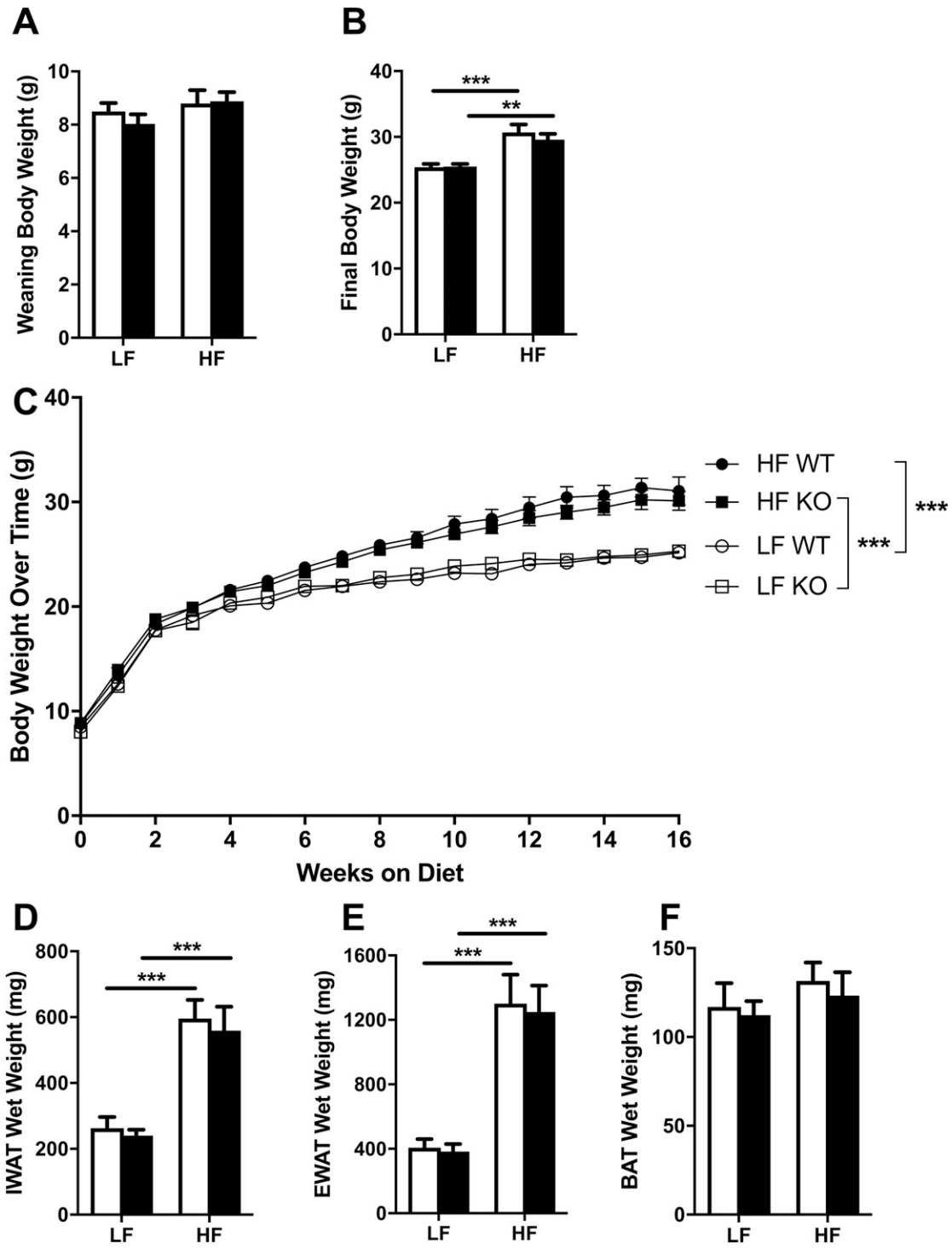

Figure 1. Body weight and adipose tissue mass. Means ± SEM; n = 9 to 10. (A–C) Body weights in WT and NLRX1 KO mice fed an LF or HF diet upon weaning (A), after 16 weeks on the diet (B), and over time (C). (D–F) Inguinal white adipose tissue (IWAT) wet weight (D), epididymal white adipose tissue (EWAT) wet weight (E), and brown adipose tissue (BAT) wet weight (F) after 16 weeks on the diet. Open columns, WT; filled columns, KO; ○, LF WT; □, LF KO; ●, HF WT; ■, HF KO. $^{**}P < 0.01$, $^{***}P < 0.001$, by two-way ANOVA, Tukey posttest.

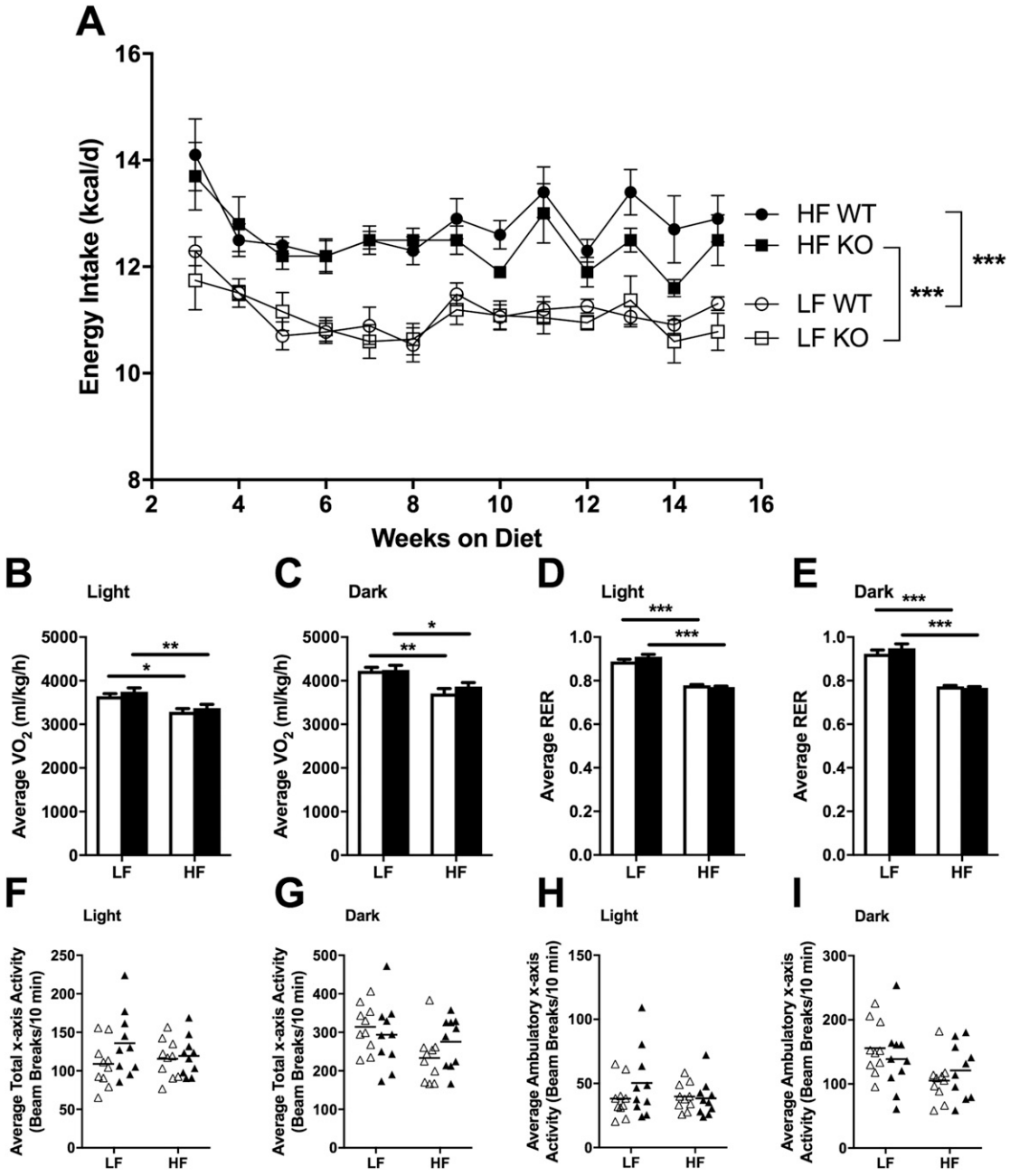

Figure 2. Energy intake, VO_2, RER, and spontaneous physical activity. Means ± SEM; n = 10. (A) Energy intake over time in WT and NLRX1 KO mice fed an LF or HF diet. (B–I) VO_2 (B and C), RER (D and E), average total *x*-axis activity (F and G), and average ambulatory x-axis activity (H and I) during the light and dark cycles after 16 weeks on the diet. ○, LF WT; □, LF KO; ●, HF WT; ■, HF KO; open bars, WT; filled bars, KO; △, WT; ▲, KO. *$P < 0.05$, **$P < 0.01$, ***$P < 0.001$, by two-way ANOVA, Tukey posttest.

was a trend for HF KO mice to have lower blood glucose compared with HF WT mice during the GTT, but this did not reach statistical significance. There was, however, a striking difference in plasma insulin levels during the GTT: HF WT mice showed an insulin peak at 15 minutes postinjection ($P < 0.05$) whereas HF KO mice did not ($F_{3,88} = 4.335$, $P < 0.01$) (Fig. 4B). HF-fed mice had poorer insulin tolerance compared with LF-fed mice ($F_{3,36} = 10.41$, $P < 0.0001$), but there were no genotype differences in insulin tolerance (Fig. 4C and 4D).

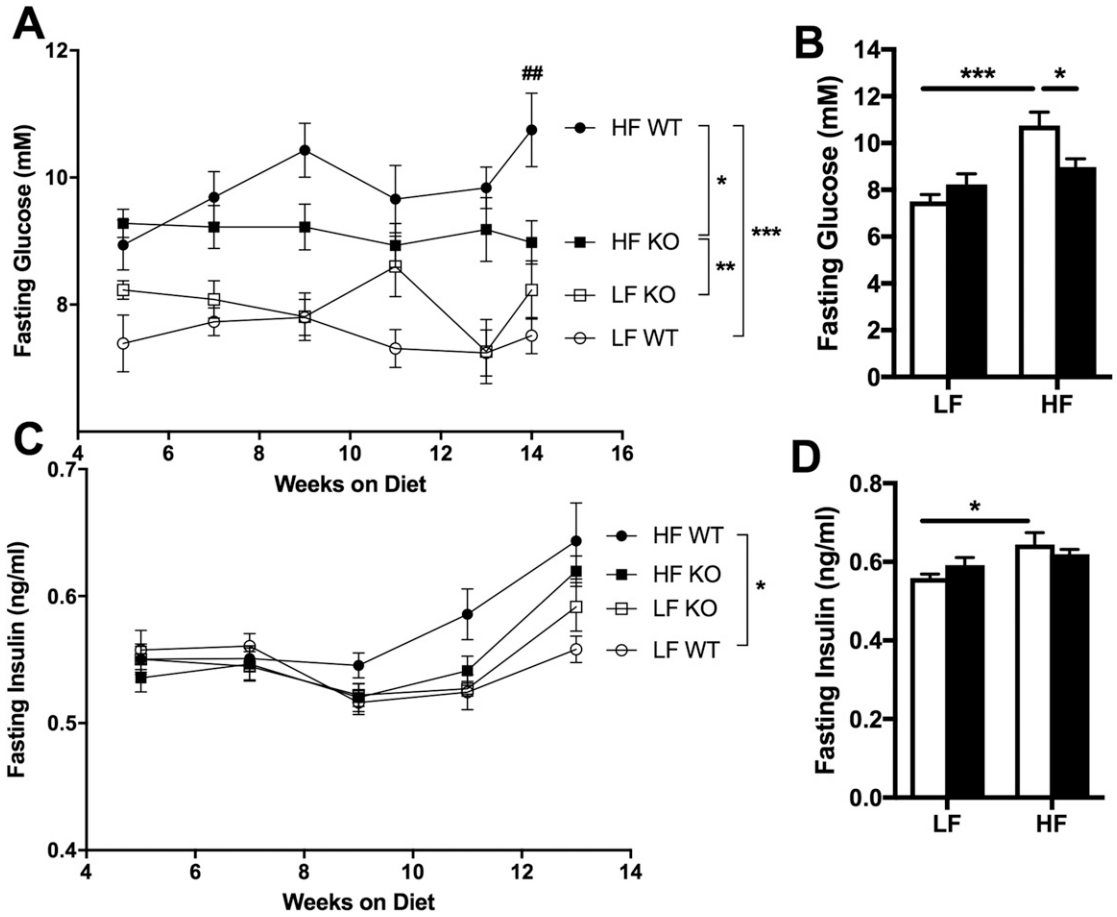

Figure 3. Fasting glucose and insulin. Means ± SEM; n=10. (A–D) Fasting blood glucose (A and B) and plasma insulin (C and D) over time (A and C) and at study endpoint (B and D) in WT and NLRX1 KO mice fed an LF or HF diet. ○, LF WT; □, LF KO; ●, HF WT; ■, HF KO; open bars, WT; filled bars, KO. $^{\#\#}P < 0.01$, HF WT vs HF KO; $^{*}P < 0.05$, $^{**}P < 0.01$, $^{***}P < 0.001$; by two-way ANOVA, Tukey posttest.

E. Pancreas

There were no genotype differences in soleus, gastrocnemius, quadriceps, liver, heart, kidney, or spleen weights (Table 1). HF WT mice had higher pancreas weights compared with LF WT mice (effect of diet: $F_{1,35} = 9.476$, $P < 0.01$), but strikingly, HF KO mice were protected from the HF-induced increase in pancreatic weight ($P < 0.05$) (Fig. 5A). Histological analysis of pancreatic sections showed that KO mice were protected ($P < 0.05$) from the accumulation of ectopic lipid in the pancreas in response to HF feeding (effect of diet: $F_{1,36} = 30.67$, $P < 0.0001$) (Fig. 5B and 5C). Despite the fact that we observed no genotype differences in insulin-positive areas of pancreatic sections (Fig. 5D and 5E), these data suggest that the metabolic response of the pancreas to overnutrition is very different in the absence of NLRX1.

3. Discussion

We originally hypothesized that the NLRX1 whole-body KO mouse would be less prone to obesity when fed an HF diet owing to our recent observations in cells lacking NLRX1 [18]. Because HF diet–induced obesity is associated with the development of insulin resistance and type 2 diabetes mellitus (T2DM) [20], we anticipated that KO mice would also be less prone to the development T2DM. We were therefore surprised to discover that HF-fed KO mice gained the same amount of weight as did HF-fed WT mice. There are several reasons why this might

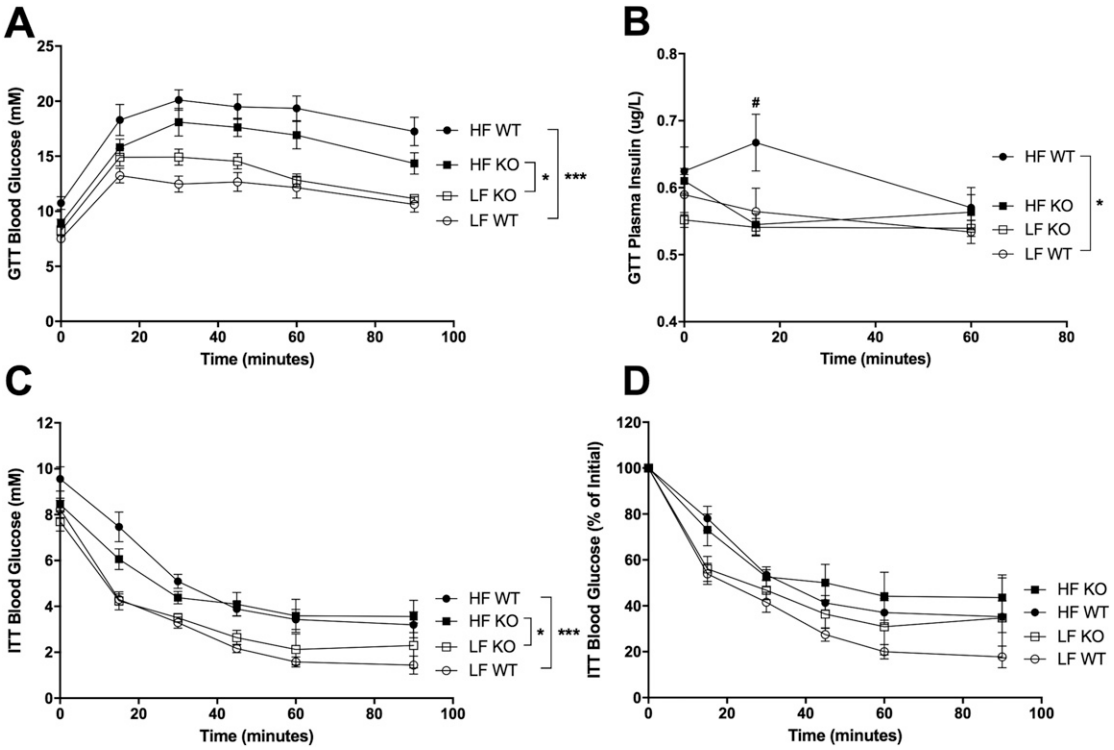

Figure 4. Glucose and insulin tolerance. Means ± SEM; n = 5 to 10. (A and B) Blood glucose (A) and plasma insulin (B) during the GTT performed on WT and NLRX1 KO mice after 14 weeks on a LF or HF diet. (C and D) Blood glucose (C) and percentage of initial blood glucose (D) during the ITT performed on WT and KO mice after 15 weeks on a LF or HF diet. ○, LF WT; □, LF KO; ●, HF WT; ■, HF KO.$^{\#}P < 0.05$ HF WT vs HF KO; $^{*}P < 0.05$, $^{***}P < 0.001$; by two-way ANOVA, Tukey posttest.

be. (1) The original NLRX1 overexpression/ablation studies were performed in mouse embryonic fibroblasts; however, NLRX1 may play a different role in embryonic development than it does in the mature organism. (2) Other mechanistic-redundant mitochondrial proteins could be compensating for the lack of NLRX1. (3) Energy regulation is an essential process for the survival of the organism; it is therefore possible that the central nervous system is

Table 1. Muscle and Organ Wet Weights

Tissue (mg)	LF WT	LF KO	HF WT	HF KO	Two-Way ANOVA	Tukey Posttest
Soleus	15 ± 2	15 ± 3	17 ± 2	18 ± 2	Effect of diet: $F_{1,36} = 16.22$, $P < 0.001$	LF WT vs HF KO, $P < 0.05$ LF KO vs HF KO, $P < 0.05$
Gastrocnemius	276 ± 20	281 ± 27	280 ± 17	289 ± 27	NS	NS
Quadriceps	323 ± 38	287 ± 29	309 ± 39	306 ± 34	NS	NS
Liver	1035 ± 116	990 ± 125	977 ± 154	962 ± 106	NS	NS
Heart	140 ± 17	144 ± 11	153 ± 13	144 ± 13	NS	NS
Kidneys	332 ± 25	333 ± 14	383 ± 66	389 ± 36	Effect of diet: $F_{1,36} = 17.6$, $P < 0.001$	LF WT vs HF WT, $P < 0.05$ LF WT vs HF KO, $P < 0.05$ LF KO vs HF WT, $P < 0.05$ LF KO vs HF KO, $P < 0.05$
Spleen	70 ± 9	96 ± 32	99 ± 36	88 ± 34	NS	NS

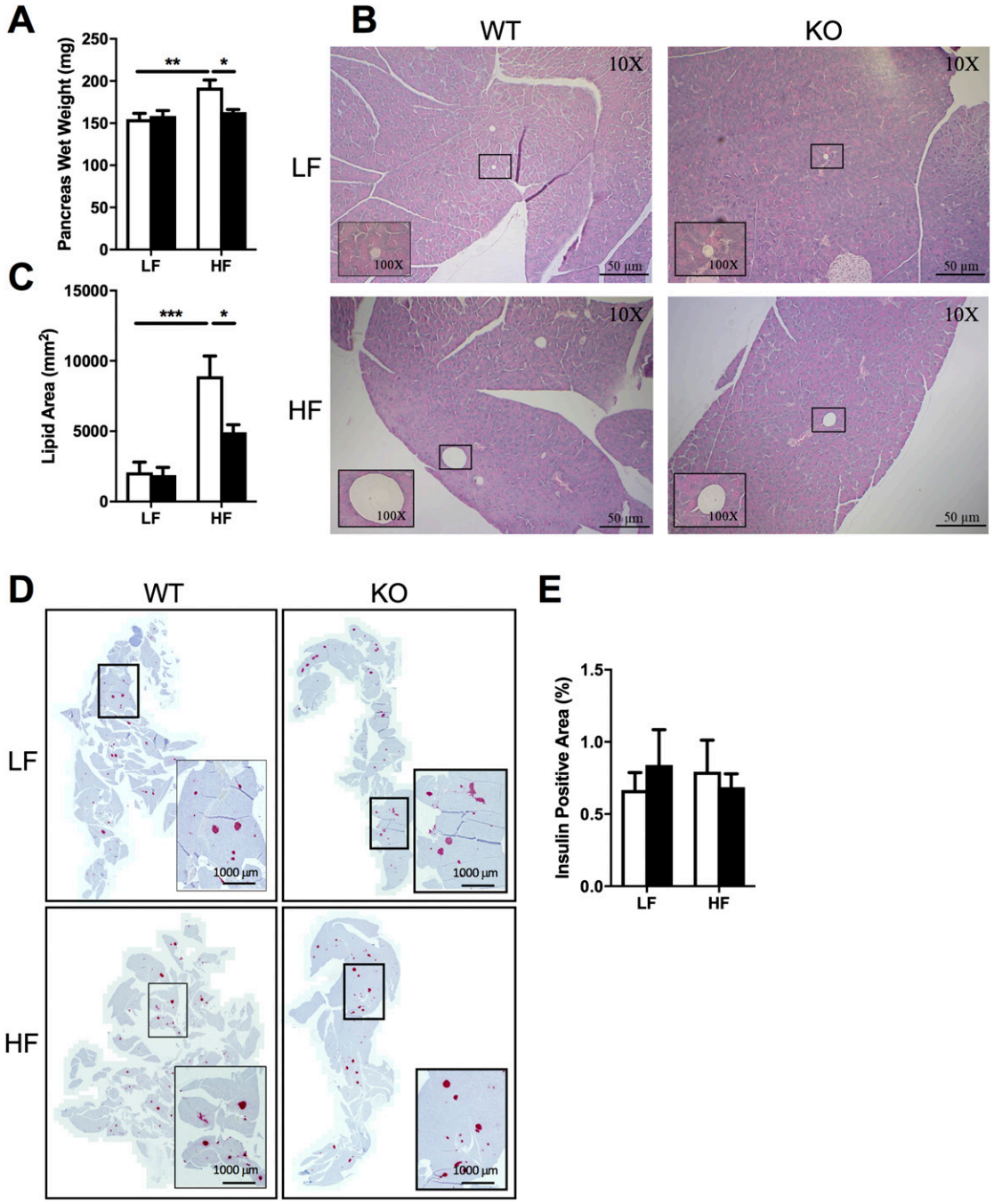

Figure 5. Pancreas weight, lipid content, and insulin content. Means ± SEM; n = 9 to 10 (A–C), n = 3 to 4 (D and E). (A–E) Pancreas wet weight (A), lipid content (B and C), and insulin content (D and E) in WT and NLRX1 KO mice fed an LF or HF diet for 16 weeks. Scale bars, 50 µm (B) and 1000 µm (D). $*P < 0.05$, $**P < 0.01$, $***P < 0.001$, by two-way ANOVA, Tukey posttest.

overriding the effects of NLRX1 ablation by activating other pathways to correct for the energy imbalance. All three of these speculations, however, will require further exploration to determine their validity.

Interestingly, although HF-fed KO mice gained as much weight as did HF-fed WT mice, they were protected from ectopic accumulation of lipid in the pancreas (Fig. 5A–5C) and were partially protected from the development of hyperglycemia (Figs. 3 and 4). This is most

evident in fasting levels of glucose measured during the course of the study: HF-fed KO mice had significantly lower fasting glucose levels compared with HF-fed WT mice (Fig. 3A and 3B). Although there was a trend for HF-fed KO mice to have lower glucose levels during the GTT, this did not reach statistical significance (Fig. 4A); however, insulin levels of HF-fed KO mice during the GTT mimicked those of LF-fed WT and LF-fed KO mice, not HF-fed WT mice (Fig. 4B). HF-fed WT mice showed a peak in insulin at the 15 minute time point whereas HF-fed KO mice did not. It is possible that the insulin peak occurred prior to the 15 minute mark in these animals and had already decreased to fasting levels (similar to the curve observed in the LF-fed mice). This would suggest that HF-fed NLRX1 KO mice are more sensitive to insulin than are HF-fed WT mice, as they were able to achieve a more profound decrease in blood glucose with less insulin compared with HF-fed WT mice. There was a trend for HF-fed KO mice to have lower levels of fasting insulin compared with HF-fed WT mice during the course of the study, but this did not reach statistical significance. Although the insulin levels of the HF-fed KO mice during the GTT hinted at improved insulin sensitivity, we observed no genotype differences in insulin tolerance during the ITT (Fig. 4C and 4D). It is possible that the dose of insulin used (2 U/kg) may have masked more subtle differences in insulin sensitivity. Future studies will aim to tease apart these potential differences by using a smaller bolus (1 U/kg) of insulin during the ITT as well as by carrying out hyperinsulinemic/euglycemic clamps, which are considered the gold standard method of evaluating insulin sensitivity.

It is well established in the literature that overnutrition leads to abnormal storage of lipid in nonadipose tissues such as skeletal muscle, liver, heart, kidney, and pancreas (reviewed in [20]). In particular, ectopic storage of lipid in the insulin-producing cells of the pancreas leads to lipotoxicity, dysfunction of the glucose-stimulated insulin secretion (GSIS) response, and eventual overt T2DM [21, 22]. Indeed, in our study we found that WT mice accumulated pancreatic lipid and demonstrated hyperglycemia, hyperinsulinemia, impaired glucose tolerance, and impaired insulin tolerance in response to HF feeding. Because ablation of NLRX1 leads to increased mitochondrial respiration but lower levels of ATP [18], we expected to observe less pronounced ectopic accumulation of lipid in KO mice in response to HF feeding and perhaps a less severe manifestation of T2DM as a result [20]. Indeed, we found that HF-fed KO mice were protected from the accumulation of pancreatic lipid despite similar body weights and levels of adiposity. To attempt to start to understand the mechanism of this result, we measured insulin-positive cells in sections of pancreata via immunohistochemistry; however, we did not find any differences in insulin staining. Note that the sample size for insulin staining of the pancreas was rather small (n = 3 to 4) due to an insufficient number of sample sections, and the current sample size may not have been large enough to detect differences. Regardless, further studies on isolated pancreatic islets will be required to determine whether NLRX1 plays a direct role in modulating GSIS. It is also important to note that we did not measure accumulation of lipid in the β cells of the pancreas directly. It will be essential to establish whether the endocrine pancreas in addition to the exocrine pancreas is indeed affected to establish a direct link to the whole-body effects observed in this model. Another measure that will be important in future studies will be the serum levels of triglyceride and free fatty acids, as these have been associated with pancreatic lipid deposition. It is curious that the pancreas should emerge as the tissue most affected by ablation of NLRX1 in a whole-body knockout model. It is possible that other mechanistic-redundant mitochondrial proteins are compensating for the lack of NLRX1 in other tissues. Further studies, perhaps in tissue-specific KO mice, will be required to understand the sensitivity of the pancreas to the presence or absence of NLRX1.

Uncoupling protein (UCP)-2 is a ubiquitously expressed mitochondrial inner membrane protein that facilitates uncoupling when activated via deglutathionylation [8]. In pancreatic β cells, activated UCP2 does not significantly affect ATP production, but instead contributes to the control of GSIS [23, 24]. Interestingly, ROS produced in the mitochondrial matrix activate UCP2 and decrease GSIS whereas ROS from the cytosol deactivate UCP2 and amplify GSIS [24]. ROS-mediated control of GSIS in β cells is clearly complex and not entirely understood. It therefore seems reasonable to hypothesize that the lack of NLRX1 in β cells might be affecting

the mitochondrial-to-nonmitochondrial ratio of ROS and potentially affecting GSIS in our mouse model. The partial protection from HF diet–induced hyperglycemia observed in the KO mice compared with the WT mice seems to suggest a pancreatic phenotype consistent with enhanced GSIS; however, further studies are necessary to start to tease apart the mechanisms underlying this interesting and unexpected phenotype. Although the mechanisms restoring glucose homeostasis remain to be elucidated, NLRX1 has emerged as a potential interesting inhibitory target for the prevention of T2DM.

Acknowledgments

We acknowledge the contributions of Stephanie Schroer-McFarland (University Health Network, Toronto, Canada) for performing the indirect calorimetry experiments, and the Toronto Centre for Phenogenomics Centre for Modeling Human Disease Pathology Services (Toronto, Canada) for processing and embedding of tissues for histology.

Financial Support: This work was supported by Canadian Cancer Society Research Institute Operating Grant 496099 (to S.E.G.) and by Banting and Best Diabetes Centre Pilot and Feasibility Grant 498820 (to S.E.G.).

Correspondence: Sheila R. Costford, PhD, Genetics and Genome Biology Program, SickKids Research Institute, Hospital for Sick Children, 686 Bay Street, Toronto, Ontario M5G 0A4, Canada. E-mail: sheila.costford@sickkids.ca; or Stephen E. Girardin, PhD, Department of Laboratory Medicine and Pathobiology, Faculty of Medicine, University of Toronto, 1 King's College Circle, Toronto, Ontario M5S 1A8, Canada. E-mail: stephen.girardin@utoronto.ca.

Disclosure Summary: The authors have nothing to disclose.

References and Notes

1. Moore CB, Bergstralh DT, Duncan JA, Lei Y, Morrison TE, Zimmermann AG, Accavitti-Loper MA, Madden VJ, Sun L, Ye Z, Lich JD, Heise MT, Chen Z, Ting JP-Y. NLRX1 is a regulator of mitochondrial antiviral immunity. *Nature*. 2008;**451**(7178):573–577.
2. Arnoult D, Soares F, Tattoli I, Castanier C, Philpott DJ, Girardin SE. An N-terminal addressing sequence targets NLRX1 to the mitochondrial matrix. *J Cell Sci*. 2009;**122**(Pt 17):3161–3168.
3. Rhee H, Zou P, Udeshi ND, Martell JD, Mootha VK, Carr SA, Ting AY. Proteomic mapping of mitochondria in living cells via spatially-restricted enzymatic tagging. *Science*. 2013;**339**(6125):1328–1331.
4. Sasaki O, Yoshizumi T, Kuboyama M, Ishihara T, Suzuki E, Kawabata S, Koshiba T. A structural perspective of the MAVS-regulatory mechanism on the mitochondrial outer membrane using bioluminescence resonance energy transfer. *Biochim Biophys Acta*. 2013;**1833**(5):1017–1027.
5. Rebsamen M, Vazquez J, Tardivel A, Guarda G, Curran J, Tschopp J. NLRX1/NOD5 deficiency does not affect MAVS signalling. *Cell Death Differ*. 2011;**18**(8):1387.
6. Echtay KS, Esteves TC, Pakay JL, Jekabsons MB, Lambert AJ, Portero-Otín M, Pamplona R, Vidal-Puig AJ, Wang S, Roebuck SJ, Brand MD. A signalling role for 4-hydroxy-2-nonenal in regulation of mitochondrial uncoupling. *EMBO J*. 2003;**22**(16):4103–4110.
7. Echtay KS, Roussel D, St-Pierre J, Jekabsons MB, Cadenas S, Stuart JA, Harper JA, Roebuck SJ, Morrison A, Pickering S, Clapham JC, Brand MD. Superoxide activates mitochondrial uncoupling proteins. *Nature*. 2002;**415**(6867):96–99.
8. Mailloux RJ, Seifert EL, Bouillaud F, Aguer C, Collins S, Harper ME. Glutathionylation acts as a control switch for uncoupling proteins UCP2 and UCP3. *J Biol Chem*. 2011;**286**(24):21865–21875.
9. Costford SR, Seifert EL, Bézaire V, F Gerrits M, Bevilacqua L, Gowing A, Harper ME. The energetic implications of uncoupling protein-3 in skeletal muscle. *Appl Physiol Nutr Metab*. 2007;**32**(5):884–894.
10. Bell EL, Klimova TA, Eisenbart J, Moraes CT, Murphy MP, Budinger GRS, Chandel NS. The Q_o site of the mitochondrial complex III is required for the transduction of hypoxic signaling via reactive oxygen species production. *J Cell Biol*. 2007;**177**(6):1029–1036.
11. St-Pierre J, Buckingham JA, Roebuck SJ, Brand MD. Topology of superoxide production from different sites in the mitochondrial electron transport chain. *J Biol Chem*. 2002;**277**(47):44784–44790.
12. Turrens JF, Boveris A. Generation of superoxide anion by the NADH dehydrogenase of bovine heart mitochondria. *Biochem J*. 1980;**191**(2):421–427.
13. Tattoli I, Carneiro LA, Jéhanno M, Magalhaes JG, Shu Y, Philpott DJ, Arnoult D, Girardin SE. NLRX1 is a mitochondrial NOD-like receptor that amplifies NF-κB and JNK pathways by inducing reactive oxygen species production. *EMBO Rep*. 2008;**9**(3):293–300.

14. Soares F, Tattoli I, Rahman MA, Robertson SJ, Belcheva A, Liu D, Streutker C, Winer S, Winer DA, Martin A, Philpott DJ, Arnoult D, Girardin SE. The mitochondrial protein NLRX1 controls the balance between extrinsic and intrinsic apoptosis. *J Biol Chem*. 2014;**289**(28):19317–19330.
15. Abdul-Sater AA, Saïd-Sadier N, Lam VM, Singh B, Pettengill MA, Soares F, Tattoli I, Lipinski S, Girardin SE, Rosenstiel P, Ojcius DM. Enhancement of reactive oxygen species production and chlamydial infection by the mitochondrial Nod-like family member NLRX1. *J Biol Chem*. 2010;**285**(53): 41637–41645.
16. Unger BL, Ganesan S, Comstock AT, Faris AN, Hershenson MB, Sajjan US. Nod-like receptor X-1 is required for rhinovirus-induced barrier dysfunction in airway epithelial cells. *J Virol*. 2014;**88**(7): 3705–3718.
17. Singh K, Poteryakhina A, Zheltukhin A, Bhatelia K, Prajapati P, Sripada L, Tomar D, Singh R, Singh AK, Chumakov PM, Singh R. NLRX1 acts as tumor suppressor by regulating TNF-α induced apoptosis and metabolism in cancer cells. *Biochim Biophys Acta*. 2015;**1853**(5):1073–1086.
18. Stokman G, Kors L, Bakker PJ, Rampanelli E, Claessen N, Teske GJD, Butter L, van Andel H, van den Bergh Weerman MA, Larsen PWB, Dessing MC, Zuurbier CJ, Girardin SE, Florquin S, Leemans JC. NLRX1 dampens oxidative stress and apoptosis in tissue injury via control of mitochondrial activity. *J Exp Med*. 2017;**214**(8):2405–2420.
19. Soares F, Tattoli I, Wortzman ME, Arnoult D, Philpott DJ, Girardin SE. NLRX1 does not inhibit MAVS-dependent antiviral signalling. *Innate Immun*. 2013;**19**(4):438–448.
20. Grundy SM. Overnutrition, ectopic lipid and the metabolic syndrome. *J Investig Med*. 2016;**64**(6): 1082–1086.
21. Unger RH, Zhou YT. Lipotoxicity of beta-cells in obesity and in other causes of fatty acid spillover. *Diabetes*. 2001;**50**(Suppl 1):S118–S121.
22. Kuzmenko DI, Klimentyeva TK. Role of ceramide in apoptosis and development of insulin resistance. *Biochemistry (Mosc)*. 2016;**81**(9):913–927.
23. Robson-Doucette CA, Sultan S, Allister EM, Wikstrom JD, Koshkin V, Bhattacharjee A, Prentice KJ, Sereda SB, Shirihai OS, Wheeler MB. β-Cell uncoupling protein 2 regulates reactive oxygen species production, which influences both insulin and glucagon secretion. *Diabetes*. 2011;**60**(11):2710–2719.
24. Mailloux RJ, Fu A, Robson-Doucette C, Allister EM, Wheeler MB, Screaton R, Harper ME. Glutathionylation state of uncoupling protein-2 and the control of glucose-stimulated insulin secretion. *J Biol Chem*. 2012;**287**(47):39673–39685.